Available online at www.sciencedirect.com
ScienceDirect
Developmental Biology 312 (2007) 157–170
DEVELOPMENTAL BIOLOGY
www.elsevier.com/developmentalbiology

Wt1 and retinoic acid signaling are essential for stellate cell development and liver morphogenesis

A. Ijpenberg [a,1,2], J.M. Pérez-Pomares [b,2], J.A. Guadix [b], R. Carmona [b], V. Portillo-Sánchez, D. Macías [b], P. Hohenstein [a], C.M. Miles [a,3], N.D. Hastie [a], R. Muñoz-Chápuli [b,*]

[a] MRC Human Genetics Unit, Western General Hospital, Edinburgh, UK
[b] Department of Animal Biology, Faculty of Science, University of Málaga, E-29071 Málaga, Spain

Received for publication 7 December 2006; revised 3 September 2007; accepted 10 September 2007
Available online 18 September 2007

Abstract

Previous studies of knock-out mouse embryos have shown that the Wilms' tumor suppressor gene (*Wt1*) is indispensable for the development of kidneys, gonads, heart, adrenals and spleen. Using OPT (Optical Projection Tomography) we have found a new role for Wt1 in mouse liver development. In the absence of Wt1, the liver is reduced in size, and shows lobing abnormalities. In normal embryos, coelomic cells expressing Wt1, GATA-4, RALDH2 and RXRα delaminate from the surface of the liver, intermingle with the hepatoblasts and incorporate to the sinusoidal walls. Some of these cells express desmin, suggesting a contribution to the stellate cell population. Other cells, keeping high levels of RXRα immunoreactivity, are negative for stellate or smooth muscle cell markers. However, coelomic cells lining the liver of Wt1-null embryos show decreased or absent RALDH2 expression, the population of cells expressing high levels of RXRα is much reduced and the proliferation of hepatoblasts and RXRα-positive cells is significantly decreased. On the other hand, the expression of smooth muscle cell specific α-actin increases throughout the liver, suggesting an accelerated and probably anomalous differentiation of stellate cell progenitors. We describe a similar retardation of liver growth in RXRα-null mice as well as in chick embryos after inhibition of retinoic acid synthesis. We propose that *Wt1* expression in cells delaminating from the coelomic epithelium is essential for the expansion of the progenitor population of liver stellate cells and for liver morphogenesis. Mechanistically, at least part of this effect is mediated via the retinoic acid signaling pathway.

Keywords: Wt1; Stellate cells; Liver development; RALDH2; Retinoic acid; RXRα

Introduction

The gene *Wt1* encodes a zinc-finger transcription factor involved in the development of several organs and in tumorigenesis. It has been experimentally demonstrated that Wt1 is able to activate and repress the transcription of many genes, but its physiological targets are still uncertain (Davies et al., 1999; Little et al., 1999). In normal development, Wt1 is transiently expressed in several mesodermal tissues, namely in mesothelial and submesothelial cells, derivatives of the intermediate mesoderm such as meso and metanephros, gonads and adrenals (Pritchard-Jones et al., 1990; Pelletier et al., 1991; Armstrong et al., 1993; Rackley et al., 1993), as well as the septum transversum and the limbs (Moore et al., 1998). *Wt1* knock-out embryos have no kidneys, gonads, spleen nor adrenal glands and die at mid-gestation due to heart abnormalities (Kreidberg et al., 1993; Moore et al., 1999; Herzer et al., 1999).

We have studied in detail the visceral phenotype of *Wt1*-null mice, and found a previously undescribed liver hypoplasia with defects in lobe formation, as well as a mal-positioning of the stomach. Interestingly, *Wt1* is expressed in the coelomic epithelium covering these viscerae, as well as in the mesenchymal

* Corresponding author. Fax: +34 952131668.
E-mail address: chapuli@uma.es (R. Muñoz-Chápuli).
[1] Present address: Institute of Stem Cell Research, GSF-National Research Center for Environment and Health, Neuherberg, Germany.
[2] Contributed equally to this work.
[3] Present address: Institute of Human Genetics, International Centre for Life, Newcastle upon Tyne, UK.

0012-1606/$ - see front matter © 2007 Elsevier Inc. All rights reserved.
doi:10.1016/j.ydbio.2007.09.014

cells that delaminate from this epithelium, invade the septum transversum and the liver primordium and contribute to the diaphragm. Using chick embryos, we have previously shown that these delaminating coelomic cells contribute to the stellate (Ito) cell population, as well as to the sinusoidal endothelium (Perez-Pomares et al., 2004). However, the origin of stellate cells in mammals remains obscure (Cassiman et al., 2006). On the other hand, the expression pattern of *Wt1* in the liver coincides with that of the main retinoic acid (RA) synthesizing enzyme RALDH2. Moreover, since RXRα-null mice also display a hitherto unexplained liver hypoplasia (Sucov et al., 1994) and equally die of cardiac failure, we suspected a functional connection between Wt1 and RA-dependent signaling.

In this paper, we present our detailed analysis of the role of Wt1 and retinoic acid signaling during early hepatic development. Our results provide new molecular evidence for parallels in visceral tissue development, whereby Wt1 expression in mesenchymal cells derived from the coelomic epithelium is essential for the development of the underlying tissue.

Material and methods

All the procedures involving use of animals were compliant with the legal regulations from the countries where these procedures were performed.

Generation of transgenic mice

Wt1 knock-out mice were generated by gene targeting, as previously described (Kreidberg et al., 1993). Embryos were genotyped by PCR on their yolk sacs. E11.5–E13.5 homozygous embryos were fully studied via serial sectioning or 3D virtual reconstruction using OPT (see below). Heterozygous and wild-type littermates were used as controls. All embryos were alive at the moment of their collection. The yWT470LacZ mouse strain (A9.3, line H) expressing LacZ under control of 470 kb of the human Wt1 locus has been previously described (Moore et al., 1999).

The RXRα knock-out mouse line was previously described (Kastner et al., 1994). We used E12.5 and E13.5 embryos for morphological comparison with Wt1-null embryos.

Histology and immunohistochemistry

For histology and immunohistochemistry, embryos were fixed in 4% buffered paraformaldehyde in PBS, in methanol-acetone-water (2:2:1) or in Dent's fixative (methanol-DMSO 4:1), dehydrated and paraffin-embedded. Some embryos were fixed through cryosubstitution, snap frozen in liquid nitrogen and kept in methanol at −80 °C for 5 days. Subsequently, the embryos were kept at −20 °C for 6 h, washed twice with methanol at 4 °C (45 min) and twice with methanol at room temperature. Dehydration was completed in methanol/butanol 1:1 (20 min) and pure butanol (20 min). yWT470lacZ Transgenic embryos were fixed o/n in 2% PFA at 4 °C. After washing in PBS, the embryos were stained with Xgal, washed and stored in 1% PFA until further use. Immunoperoxidase and double immunofluorescence staining were performed as previously described (Guadix et al., 2006).

The monoclonal mouse anti-smooth muscle cell (SMC) α-actin antibody (clone 1A4, Sigma) was used at a 1:2000 dilution for immunoperoxidase staining and at 1:100 for immunofluorescence. Polyclonal rabbit anti-RALDH2 (a gift of Dr. Peter McCaffery, Eunice Shriver Center, University of Massachusetts) was used at a 1:5000 dilution. Polyclonal rabbit anti-RXRα (Sc-553, Santa Cruz) and anti-HNF1 (Sc-8986, Santa Cruz) were used at a 1:300 and 1:400 dilutions for immunoperoxidase, respectively, or at a 1:100 for immunofluorescence. For RXRα immunofluorescence, tyramide signal amplification (TSA Kit, Perkin-Elmer) was necessary. Monoclonal mouse anti-desmin (clone DE-U-10, Sigma) was used at 1:200 for immunoperoxidase and 1:100 for immunofluorescence. Polyclonal goat anti-GATA-4 (Sc-1237, Santa Cruz) was used at 1:50 dilution for immunoperoxidase and, with tyramide amplification, for immunofluorescence. Polyclonal rabbit anti-phosphohistone H3 (#06-570, Upstate) was used at a 1:200 dilution. Monoclonal rat anti-Ter119 (Sc-19952, Santa Cruz), monoclonal mouse anti-PCNA (Sigma) and polyclonal rabbit anti-bovine epidermal cytokeratin (Z622, Dakopatts, Denmark) were used at 1:100 dilution.

OPT analysis

Wt1 wild-type and null embryos for morphological analysis were fixed for 2 h in 4% PFA at 4 °C. The embryos were dehydrated using sequential MeOH/PBS wash steps (25%, 50%, 75%), and stored in 100% MeOH at −20 °C until further use. Before OPT embedding (see below), the embryos were slowly rehydrated using several wash steps.

All embryos were embedded in 1% low-melting point agarose, immersed in Murray's Clear, and scanned through 360° as previously described (Sharpe et al., 2002). Morphological differences between Wt1 wild-type and mutant embryos were detected by scanning for the auto-fluorescence emitted by all tissues. Using a back-projection algorithm, the 400 captured digital images were independently reconstructed, and high-resolution representations of sections through the specimen were produced. Alternatively, 3D iso-surfaces (contours that connect all regions above a certain threshold intensity) were generated to illustrate the shapes of the tissues in which they were expressed.

Image analysis

Co-localization analysis using confocal images was performed through image processing with ImageJ software. Briefly, we obtained images composed of the non-black pixels present at the same time in the red and green channels as previously described (Carmona et al., 2007). Quantification of the signal in these and other immunoperoxidase images was also performed with ImageJ software. Comparisons were always made on equivalent images, obtained during the same experiment and captured under the same conditions. A gray level threshold was manually established for the selection of the positive cells, and the same threshold was applied to all the images. Then, the surface of the selected cells was measured and expressed as percentage of the total surface. Comparison of mean values for each group of measurements was made using the Student's *t*-test.

RALDH2 inhibition and in vitro culture of quail liver explants

RA-synthesis was inhibited by two competitive inhibitors of aldehyde dehydrogenases, DEAB (4-diethylaminobenzaldehyde, Sigma) and citral (Fluka). Stock solutions were made in DMSO (DEAB, 150 mM; citral, 100 mM). For injection, the competitive inhibitor stocks were further diluted with Tyrode solution to obtain a final concentration of 0.4 mM.

Chick eggs were incubated for 48–72 h. After windowing, 2 ml of albumin was aspirated, after which 2 ml of either DEAB or citral solution was injected per egg. The eggs were re-incubated for 24 h. Then, a further 1 ml of the inhibitor solution was injected into the egg, after which it was incubated again for 24 h. Control eggs were injected with the same volume of DMSO diluted 1:250 with Tyrode.

In order to check the effects of RA and RA inhibitors on *in vitro* growth of liver explants, we dissected the hepatic primordia of HH16-HH17 quail embryos, and we cultured them in four-well plates (Nunc) with DMEM (Gibco) supplemented with 10% fetal bovine serum (Paa), 2% chick serum (Sigma), 100 IU penicillin/streptomycin (Gibco) and Plasmocin (Invivogen) at 37 °C, 5% CO_2. Two explants were placed in each well and treated with 10 μM citral, 1 μM RA, both substances or vehicle (DMSO) only. After 24 h, the explants from each well were pooled and trypsinized, and the cells were pelleted, washed twice in cold PBS+0.1% fetal bovine serum, fixed in ice-cold 70° ethanol for 1 h, washed again in PBS, treated with 100 μg/ml Rnase-A and stained with propidium iodide (40 μg/ml) for 1 h at 37 °C. Cell fluorescence was analyzed using a MoFlo flow cytometer and the results were quantified with Summit 4.0 software. The experiment was performed by duplicate.

Results

Anatomy of the liver and stomach in Wt1-null mice

In Wt1-null embryos, the liver shape and size are grossly abnormal by E13.5 (Figs. 1A–H). In wild-type embryos, the liver is divided into three main lobes, one of them surrounding the stomach dorsally and covering most of the greater curvature of the gastric wall (Figs. 1A, C). The entire surface of the diaphragm (transverse septum and pleuroperitoneal septa) is in contact with the liver. Instead, in the mutant embryos, the liver was much smaller and attached only to the apex of the transverse septum and the right surface of the mesogastrium. Pleuroperitoneal septa were lacking, causing a mal-development of the diaphragm and a wide communication between the pleural and peritoneal cavities (Figs. 1F, I and 2). Furthermore, a clearly defined dorsal left lobe of the liver was not observed (Figs. 1B, D, F). Instead an unusual ventral lobe was observed extending to the left, ventrally to the stomach (Fig. 1B). Virtual 3D surface reconstruction of the isolated visceral organs from E13.5 wild-type (Fig. 1E) and Wt1-null (Fig. 1F) embryos clearly shows the liver hypoplasia and lobing abnormalities.

The stomach and the lesser and greater gastric omenta showed a different anatomical arrangement in the Wt1-null embryos as compared to control embryos. In the latter, a sagittally arranged omental bursa was located between the stomach and the liver (Fig. 1C). The tissue of the dorsal and ventral pancreatic buds was observed within the mesenteric tissue, to the right of the stomach. Instead, in the Wt1-null mice, the stomach was displaced dorsally and toward the left, and rotated such that the cardiac and pyloric portions were closely located (Figs. 1C, D). The omental bursa was also misplaced, covering the stomach dorsally. Due to this mal-rotation, the greater omentum was very elongated and thinned, populated by fewer mesenchymal cells and vascularized less than in the control embryos (Fig. 1D). In some cases, the dorsal pancreatic primordium could be seen extending ectopically along the greater omentum (not shown). On the other hand, α-actin smooth muscle immunoreactive cells were dispersed, and the muscular band of the stomach was poorly defined (Figs. 1C, D).

Expression of coelomic and differentation markers in the liver of control and Wt1-null mice

The yWT470LacZ mice express β-galactosidase under control of the human Wt1-promoter. By E12.5, LacZ staining was observed in the coelomic epithelium covering the liver, and also in the cells apparently migrating into the liver from the surface (Figs. 1I, J). These LacZ-positive cells are seen in the walls of the developing sinusoids, both at endothelial and subendothelial level.

No differences in hepatoblast density were observed between Wt1-null and control embryos, as shown by HNF1 staining (Figs. 3A, B). The density of erythroblasts was similar by E12,5 (not shown), but the number of erythroblasts was dramatically reduced in Wt1-null mice by E13.5 (Figs. 3C, D). Desmin immunoreactive cells were observed around the sinusoidal spaces in both Wt1-null and control embryos, without significant differences between them (Figs. 3E, F). However, we found differences in the staining pattern of SMC α-actin, which was weak and restricted to the walls of the large vessels in E12.5 and E13.5 control embryos, but widely extended, even in isolated cells, in Wt1-null embryos of the same ages (Figs. 3G, H and 6E–J). In the control embryos, coelomic cells lining the liver surface were GATA-4-positive, as well as cells apparently delaminating from the surface and interspersed between the hepatoblasts. In Wt1-null embryos, these cells were less abundant at the surface of the liver, and they were mainly located in the sinusoidal walls. GATA-4 submesothelial cells were cytokeratin immunoreactive, suggesting that they originate by delamination from the epithelial layer (Figs. 3K, L). GATA-4/desmin co-localization was also observed, although in a different pattern between Wt1-null and control embryos. In the latter, only a fraction of GATA-4 cells were also desmin immunoreactive (Figs. 3M, N). However, in Wt1-null embryos, most of the GATA-4-positive cells were located in the sinusoidal wall and expressed desmin (Figs. 3O, P).

Cell proliferation in the liver of control and Wt1-null mice

No significant differences were found in the number of proliferating cells between Wt1-null and control embryos by phosphohistone-3 immunolocalization (Figs. 4I, J). However, HNF1/PCNA co-localization showed that by E12.5 nuclei from hepatoblasts were more frequently and intensely stained with anti-PCNA antibody in control embryos (Figs. 4A–D). “Hot spots” of proliferating hepatoblasts were abundant in the surface of the liver, especially in the tips of the lobes. Through image analysis, we quantified this difference which resulted to be statistically significant ($p<0.05$) (Fig. 4K). The difference in hepatoblast proliferation rates was confirmed by cytokeratin/PCNA co-localization (not shown). On the other hand, we assessed through a similar procedure the differences in the proliferation rates of the RXRα-expressing population between Wt1-null and control embryos (Figs. 4E–H and K). By E12,5, the higher proliferation rates found in the control embryos were statistically significant ($p<0.05$). RXRα proliferating cells were most abundant in the surface of the liver (Figs. 4E, G). Highly expressing RXRα cells interspersed between the hepatocytes usually showed also high levels of PCNA immunoreactivity. Differences between Wt1-null and control embryos were smaller when considering together 12.5 and E13.5 embryos. This difference was very close to the critical values of the statistical significance ($p<0.06$).

RXRα and RALDH2 immunoreactivity in control and Wt1-null embryos

Liver RXRα immunoreactivity revealed differences between Wt1-null embryos and their control littermates (Figs. 5A–D). Both E12.5 and E13.5 control embryos showed a number of immunoreactive cells scattered between the hepatoblasts and frequently in contact with the sinusoidal walls. However, control embryos always showed more intensely stained cells not asso-

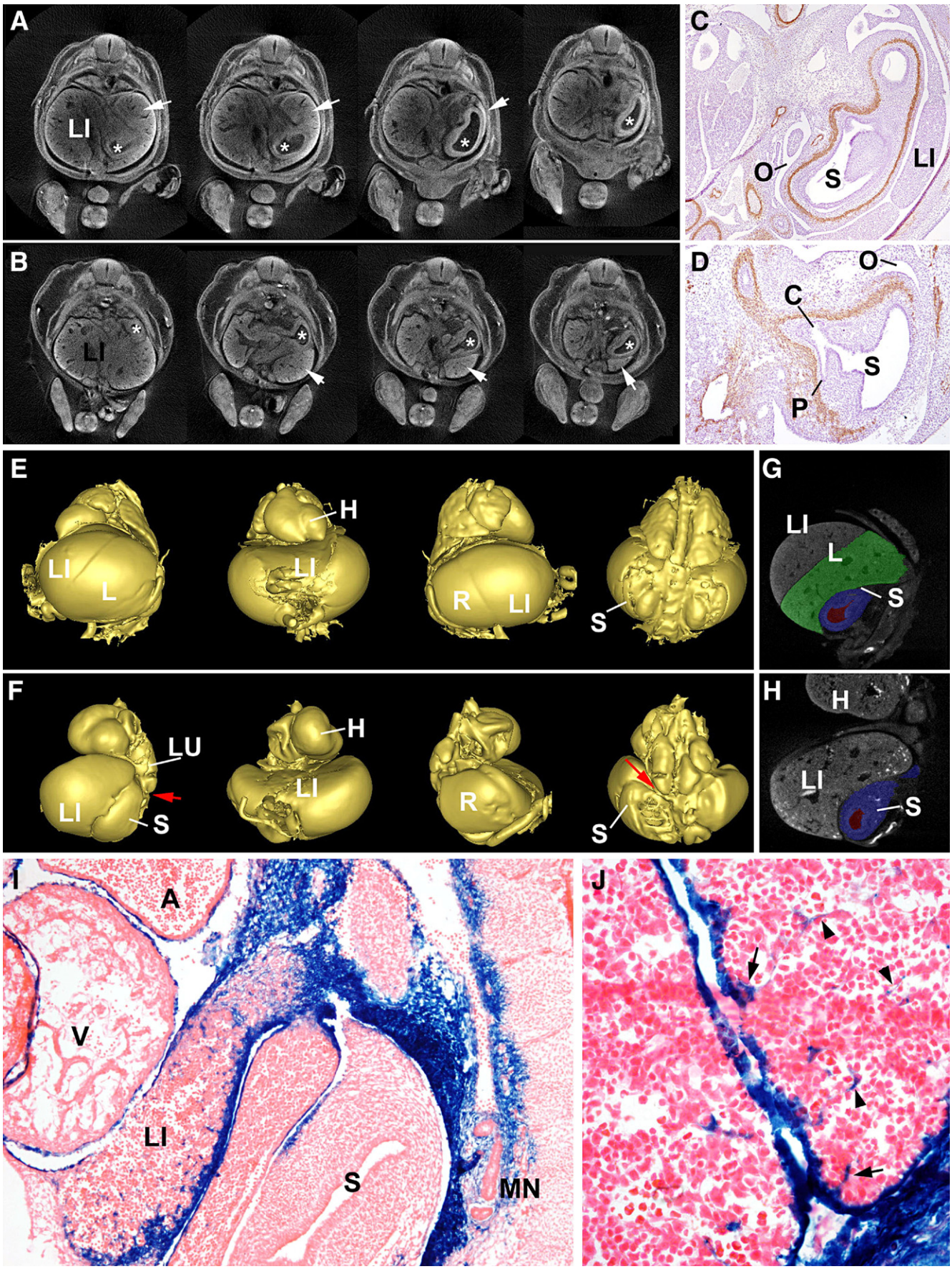
A
LI
B
LI
C
O
S
LI
D
O
C
S
P
E
LI
L
H
LI
R
LI
S
F
LU
LI
S
H
LI
R
S
G
LI
L
S
H
H
LI
S
I
A
V
LI
S
MN
J

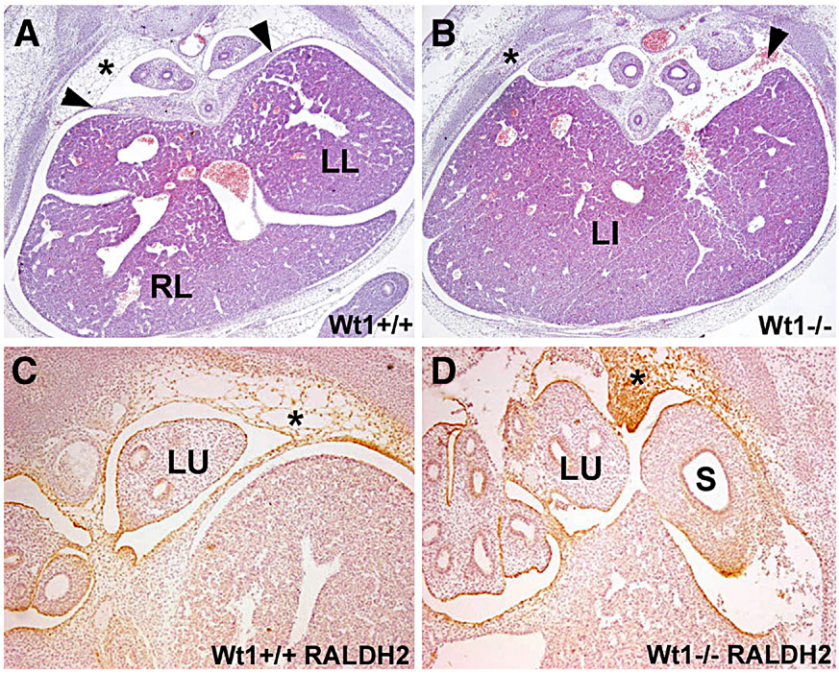

Fig. 2. Diaphragmatic defect in Wt1-null embryos. In E13.5 control embryos (A, C), the pleuroperitoneal septa are well developed (arrowheads). However, these septa are lacking in Wt1-null embryos (B, D), thus the pleural and the peritoneal cavities remain connected, allowing for contact between the left lung (LU) and the stomach (S). On the other hand, the lateral areas of the pleural cavities, which show loose tissue in normal embryos, are abundantly populated by RALDH2-positive cells in Wt1-null embryos (asterisks).

ciated with the sinusoids (Figs. 5A, B, E, F, I). RXRα staining in Wt1-null embryos was always less intense, and the RXRα-positive cells were usually located in the sinusoids (Figs. 5C, D, G, H, J). The difference in the amount of highly stained cells was statistically significant ($p<0.05$, Fig. 4K). In control embryos, RXRα expression co-localized with SMC α-actin expression in the walls of the large vessels. In contrast, in Wt1-null embryos, co-localization was observed in many cells either associated to the vessels, sinusoids or even in isolated cells (Figs. 5H and J, respectively). The RXRα signal did not co-localize with the erythroblastic marker Ter119 (Fig. 5L).

RALDH2 expression was detected by immunohistochemistry in the livers of Wt1-null and control embryos aged E10.5 and older (Figs. 2 and 6). No conspicuous differences were found in the liver of E10.5 embryos, which showed a weak immunoreactivity in the dorsal surface. However, RALDH2-positive cells were seen extending in the body wall at both sides of the dorsal coelomic cavity in control embryos, while in Wt1-null embryos these cells remained closely compacted in the same area, not extending ventrally (Figs. 6A–C). Between E11.5 and E12.5, RALDH2 immunoreactivity in control embryos was prominent throughout the liver coelomic epithelium, but more weakly in the ventral areas (Figs. 6D, E, G). Some subepithelial cells were also weakly stained, mainly in the dorsal tips of the liver lobes. Expression was also found in the dorsal and dorsolateral coelomic epithelium, as well as in the mesenchymal cells from the coelomic wall. These immunoreactive mesenchymal cells extended toward the lateroventral body wall from E10.5 to E11.5 (Figs. 6A, D, E). RALDH2 immunoreactivity decreased by E13.5, but remained detectable throughout the liver coelomic epithelium, as well as in the adjacent parietal coelomic epithelium (Figs. 6K, L). In the liver of E11.5–E13.5 Wt1-null embryos, RALDH2 immunoreactivity was always weaker than in control littermates, and it remained mainly restricted to the dorsal areas. Very weak or no immunoreactivity was found in the lateral and ventral areas of

Fig. 1. Visceral anomalies in Wt1-null embryos. (A, B) Serial virtual sections showing the anatomical arrangement of liver (LI) and stomach (asterisk) in control (A) and Wt1-null (B) E13.5 embryos. The upper row shows the normal arrangement of the left liver lobe (arrows) surrounding most of the stomach. The bottom row shows the dorsal displacement of the stomach and the presence of an abnormal liver lobe ventral to the stomach (arrows). (C, D) Transverse sections of the stomach (ST) in control (C) and Wt1-null (D) E13.5 embryos. Smooth muscle cell α-actin immunostaining. The left liver lobe (LI) is shown in the control embryo. The different location of the omental sac (O) indicates a severe malrotation of the stomach in Wt1-null mice, where cardiac (C) and pyloric (P) portions are closely located. (E, F) 3D virtual representation of the viscerae in control (E) and Wt1-null (F) E13.5 embryos. Left, front, right and rear views are shown. Left and right (L and R) lobes of the liver (LI) are indicated. Note the lack of left lobe, the smaller liver and the contact between left lung and stomach (arrows) in the WT1-NULL embryo due to the diaphragmatic defect. (G, H) Virtual sagittal sections of the viscerae of 13.5 control (G) and Wt1-null (H) embryos. Left liver lobe (L) is lacking in the Wt1-null embryo. Note the spongy appearance of the liver. H=heart. (I, J) LacZ staining in an E12.5 y470WtLacZ embryo, general view (I) and detail of the liver (J). Wt1 expression is detected in the coelomic epithelium of the atrium (A), ventricle (V) and liver. Expression is also strong in the mesonephros (MN) and around the large vessels of this area. In the liver, cells expressing the transgene can be seen in the coelomic epithelium, in cells showing signs of delamination (arrows) and also close to the sinusoidal walls (arrowheads).

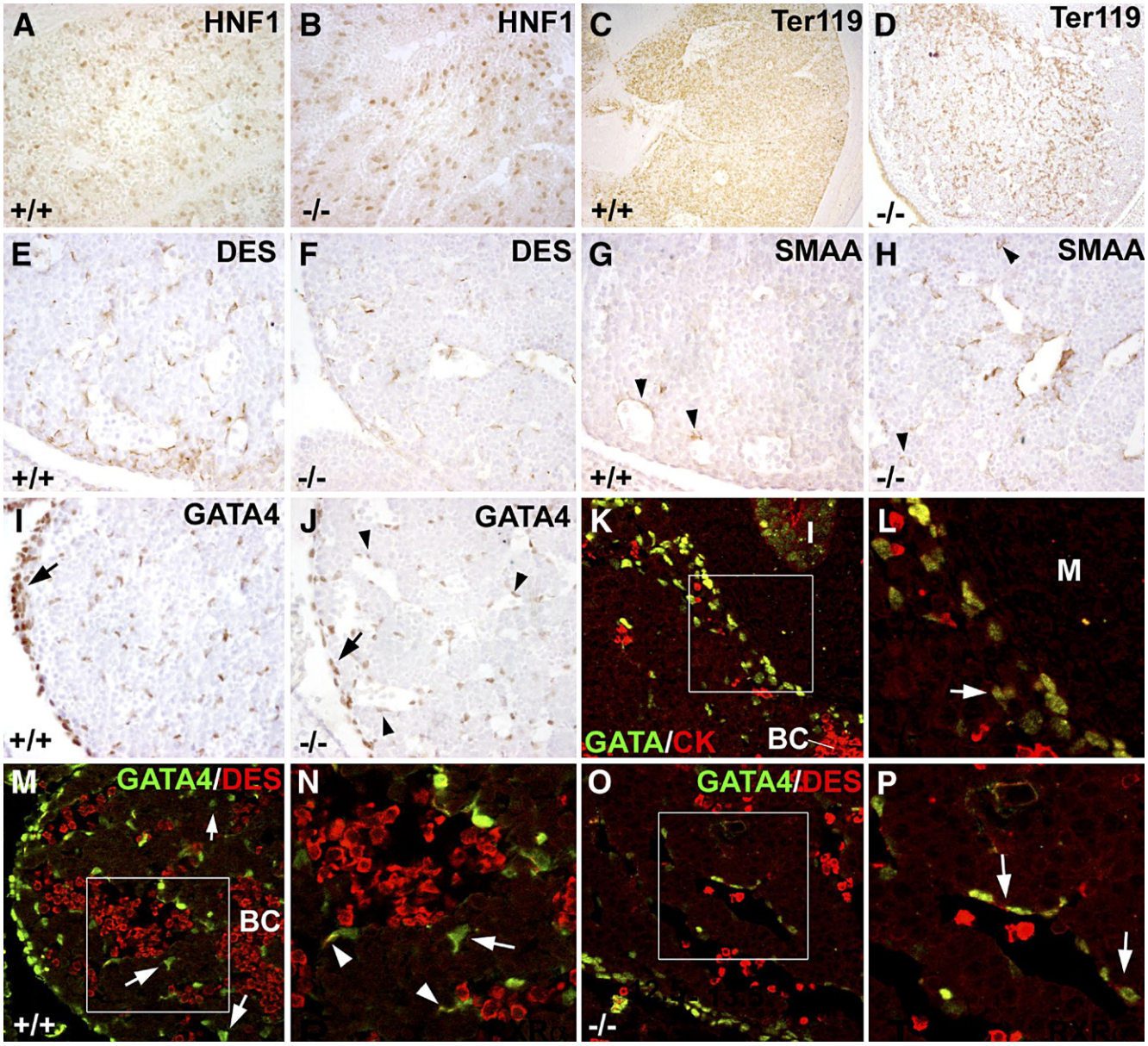

Fig. 3. Immunohistochemical analysis of livers from Wt1-null and control embryos. (A, B) Immunolocalization of the hepatoblast factor HNF1 in the liver of E12.5 control (A) and Wt1-null (B) embryos. No differences are found in the density of hepatoblasts. (C, D) Immunolocalization of the erythroblast antigen Ter119 in E13.5 control (C) and Wt1-null (D) embryos. A strong depletion of erythroblasts is evident in the mutant mice. (E, F) Desmin immunoreactive cells are present in E12.5 control (E) and Wt1-null (F) embryos, most of them can be seen in the sinusoidal walls. (G, H) SMC α-actin immunoreactive cells are scarce in control embryos of E12.5 (G), and most of them are located in the large vessel walls. SMC α-actin immunoreactivity is higher in Wt1-null embryos of the same age (H), even in cells not located close to the sinusoids (arrowheads). (I, J) The coelomic epithelium of the liver is GATA-4 immunoreactive in these E12.5 embryos, as well as the subepithelial cells and a number of cells in the liver parenchyma. Note the larger number of subepithelial cells in the control embryos (arrows) and the frequent localization of the GATA-4-positive cells in the sinusoidal walls from the Wt1-null embryos (arrowheads). (K, L) Co-localization of GATA-4 (green) and the coelomic epithelium marker cytokeratin (red) in the subepithelial cells (arrow in panel L) of an E11.5 control embryo. Note the GATA-4/cytokeratin co-localization in the intestinal epithelium (I), while the intestinal mesenchyme (M) is negative. Blood cells (BC) are auto-fluorescent. (M–P) Co-localization of GATA-4 (green) and the stellate cell marker desmin (red) in E13.5 embryos. Blood cells are auto-fluorescent. In control embryos (M, N), double stained cells can be seen in the sinusoidal walls (arrows), while other GATA-4 cells are desmin-negative (arrowheads). However, in Wt1-null embryos, most of the GATA-4 cells are in the sinusoids and express desmin (arrows).

the liver by these stages (Figs. 6F, H–J, M). This lack of immunoreactivity was uniform throughout the liver. The parietal area of immunoreactivity remained restricted at the same level as it was found by E10.5, never extending to the lateral body wall (Figs. 6C, F and insert in M). By E13.5, strongly RALDH2-positive cells accumulate in the area where the pleuroperitoneal septum defect occurs (Fig. 2D).

Liver development in RXRα-null mice

As compared to control littermates, RXRα-null embryos showed a reduced liver size, similar to Wt1-null mice (Fig. 7). The left liver lobe was small and did not surround the greater curvature of the stomach (Figs. 7C, F). The stomach was displaced to the left due to the reduction in size of the left

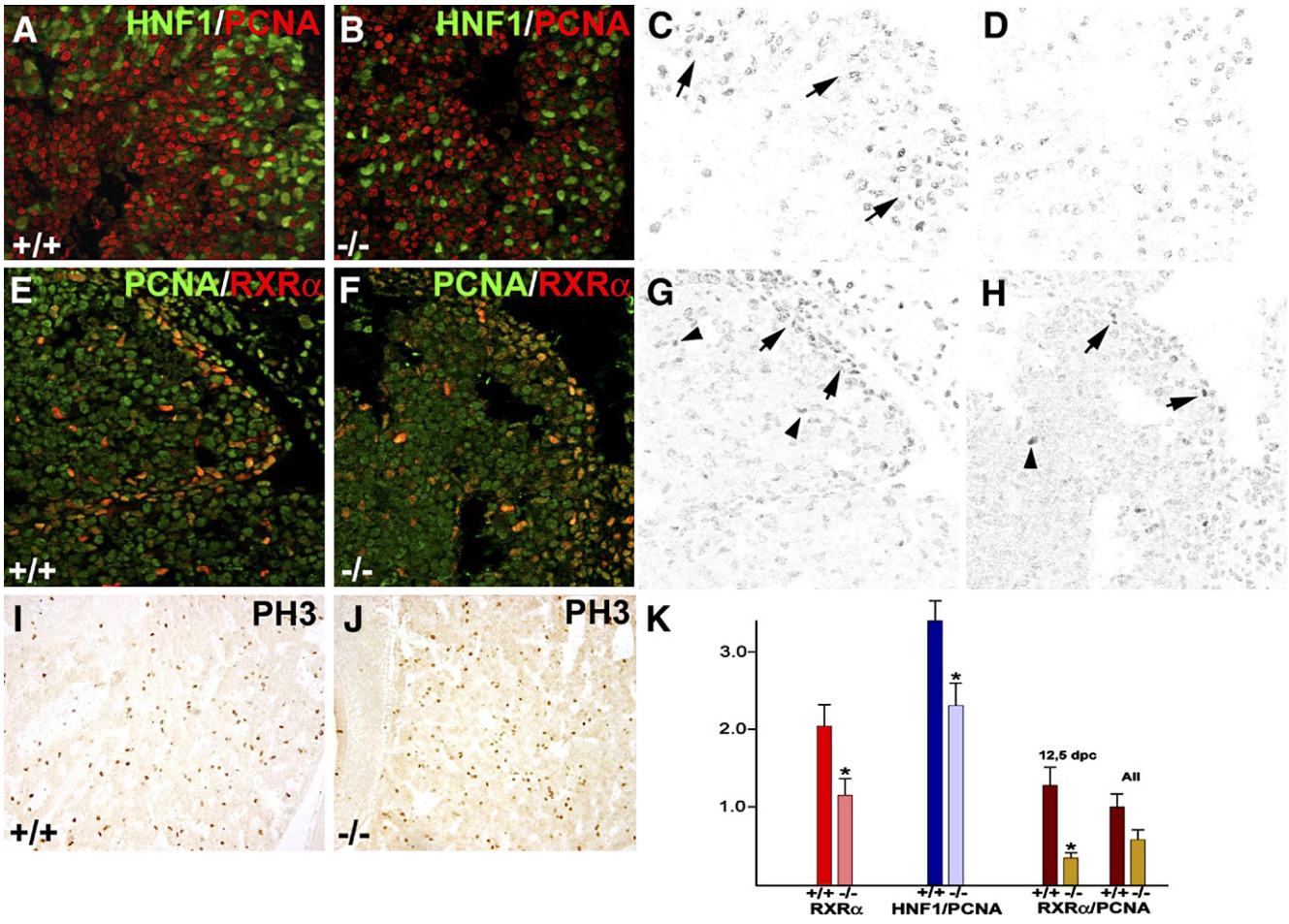

Fig. 4. Proliferation in the liver of Wt1-null and control embryos. (A, B) Co-localization of the hepatoblast marker HNF1 (green) and the proliferating cell nuclear antigen (PCNA, red) in the liver of E12.5 control (A) and Wt1-null (B) embryos. (C, D) Image of the specific HNF1/PCNA co-localization obtained through processing of images A and B and composed of the non-black pixels coinciding in the red and green channels. Panel C shows a larger number of nuclei and a higher intensity of staining than panel D, suggesting a faster proliferation of hepatoblasts in control than in Wt1-null embryos. (E, F) Co-localization of RXRα (red) and the proliferating cell nuclear antigen (PCNA, green) in the liver of E12.5 control (A) and Wt1-null (B) embryos. (G, H) Image of the specific RXRα/PCNA co-localization obtained by processing of images E and F as described above. Co-localization is more intense and frequent at the liver surface of control embryos (arrows). (G, H) Phosphohistone-3 immunoreactivity in the liver of E13.5 control (I) and Wt1-null (J) embryos. No significant differences can be seen. (K) Results of the quantitative image analysis of the RXRa immunoreactivity and the HNF1/PCNA and RXRα/PCNA co-localizations. The results are expressed as percentage of the image area. Wt1-null embryos show fewer cells expressing high levels of RXRα, less HNF1/PCNA co-localization and less RXRα/PCNA co-localization (statistically significant only in E12.5 embryos) (*$p<0.05$, Student's t test).

liver lobe, but it was not mal-rotated as in Wt1-null embryos. There was no diaphragmatic defect, but the pleuroperitoneal septa were much shorter than in controls, and the diaphragmatic muscle fibers appeared disorganized (Figs. 7B, E). SMC α-actin staining was similar in control and RXRα-null embryos.

Liver phenotype after RALDH2 inhibition

To analyze whether the observed reduction of RALDH2 expression in Wt1-null embryos is an indirect effect of the loss of Wt1 expression or whether it is causal to the phenotype, we decided to mimic loss of RALDH2 expression *in vivo* using chemical inhibitors of RA synthesis and chick embryos. RALDH2 inhibition with DEAB caused a reduction in liver size ranging from mild to severe when compared to vehicle-treated control embryos (Figs. 8A–F). In general, the strongest effects were observed in chick embryos treated between HH14 and HH15. These embryos showed extreme reduction of the liver tissue, in some cases showing only a few clusters of hepatoblasts surrounded by large hepatic sinusoids (Figs. 8B, D). No morphological signs of apoptosis or necrosis were found in the liver tissue. In embryos treated by HH16–17, the reduction in liver size was much less apparent, although livers were usually smaller than those from control embryos at the same developmental stage (Figs. 8E, F). Embryos treated by HH18–19 with the same concentrations of inhibitors showed no apparent defects in the liver nor in other embryonic areas. Besides the liver hypoplasia, the embryos looked basically normal, except for a thin ventricular myocardium (Fig. 8B). Citral-treated embryos showed the same phenotype as described for DEAB (Figs. 8G–H).

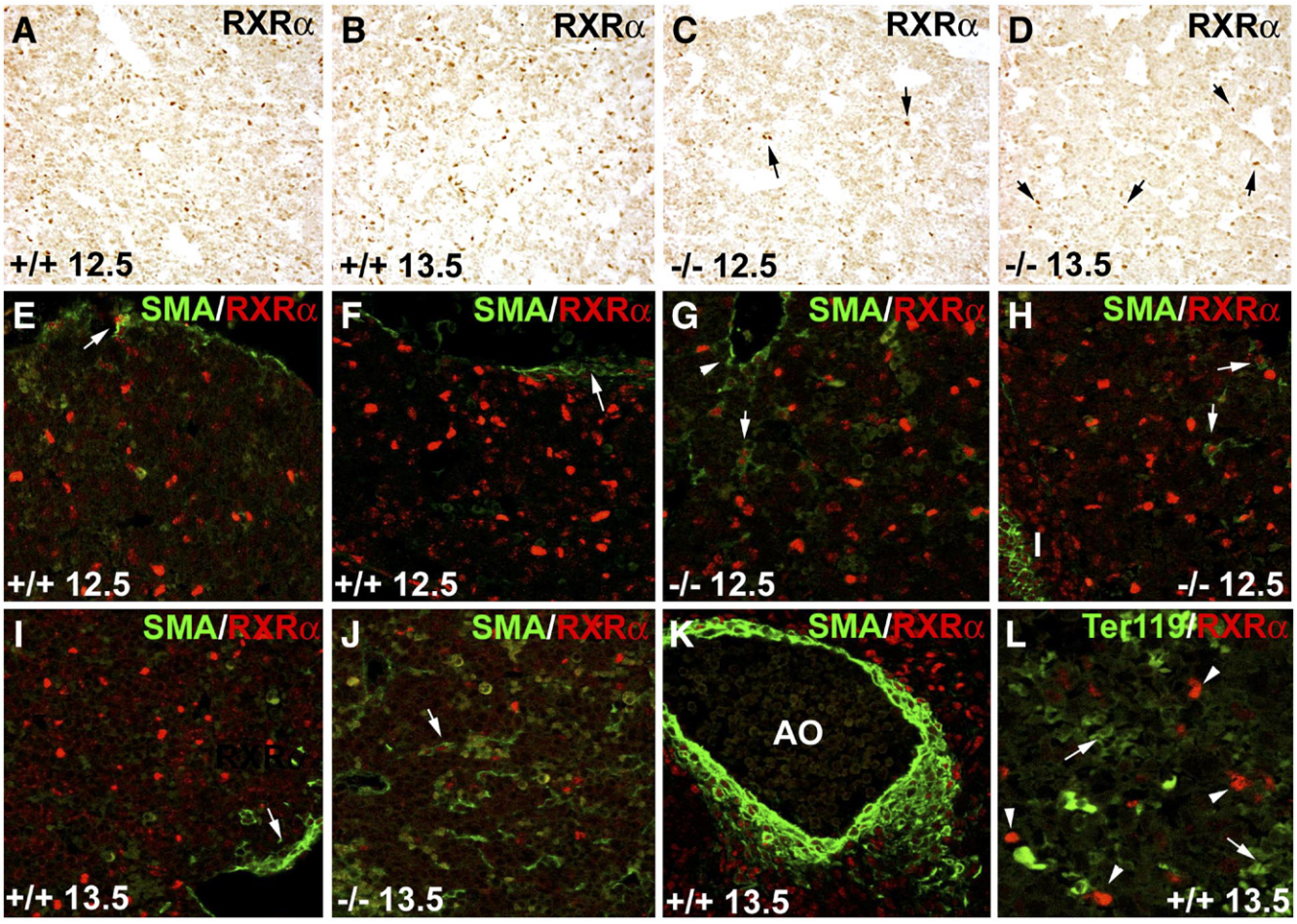

Fig. 5. RXRα expression and RXRα/SMC α-actin co-localization in the liver of Wt1-null and control embryos. (A, B) RXRα expression in the liver of E12.5 and E13.5 control embryos, respectively. (C, D) RXRα expression in the liver of E12.5 and E13.5 Wt1-null embryos, respectively. The number of highly immunoreactive cells is clearly reduced in Wt1-null embryos (arrows). (E, F) RXRα/SMC α-actin co-localization in the liver of two E12.5 control embryos. Double-stained cells are observed only in the walls of large veins (arrows). (G, H) RXRα/SMC α-actin co-localization in the liver of two E12.5 Wt1-null embryos. In both cases, double-stained cells can be seen not associated to vessels or sinusoids (arrows). Note the double-stained cells in the intestinal musculature (I). (I, J) RXRα/SMC α-actin co-localization in the liver of E13.5 control (I) and Wt1-null (J) embryos. The same features described for the E12.5 embryos can be seen, although the SMC α-actin immunoreactivity has increased in the E13.5 Wt1-null embryo. (K) Dorsal aorta from the same section where the figure I was obtained, as a positive control of the SMC α-actin immunostaining. (L) RXRα-positive cells (arrowheads) show no expression of the erythroblast marker Ter119 (arrows).

Effects of citral and RA treatment of quail liver explants on cell proliferation

Quail liver explants obtained from HH16–17 embryos showed reduced proliferation rates when cultured for 24 h only with medium (Fig. 8). The subG1 fraction was prominent, suggesting extensive cell apoptosis in addition to the cell death induced by the dissection procedure. In fact, a control experiment performed in parallel with cultured cells showed no increased subG1 fraction (not shown). Citral treatment of explants did not produce significant variations with respect to the control. However, 1 μM RA, either alone or combined with citral, leads to a 35–40% increase in cell proliferation (see table in Fig. 8). Furthermore, retinoic treatment apparently improved survival of cells in the explants, since the subG1 fraction was clearly smaller in the explants treated with RA.

Discussion

The liver is an organ formed by complex interactions between endodermal and mesodermal cells. Hepatoblasts and bile duct cells are endodermal in origin, while the sinusoidal endothelium and the stellate (Ito) cells differentiate from the mesodermal mesenchyme. Several studies, both in avian (Le Douarin, 1975; Perez-Pomares et al., 2004) and in mammalian embryos (Moore et al., 1998), have shown that at least part of the liver mesenchyme originates from the delamination of cells from the coelomic epithelium covering the liver primordium. In this study, we characterized the cells that delaminate from the hepatic coelomic epithelium and provide evidence of their contribution to the stellate cell population.

Our detailed analysis has revealed a so far unnoticed hepatic phenotype in Wt1-deficient embryos, affecting not only the size of the liver but also the anatomical arrangement of the liver and

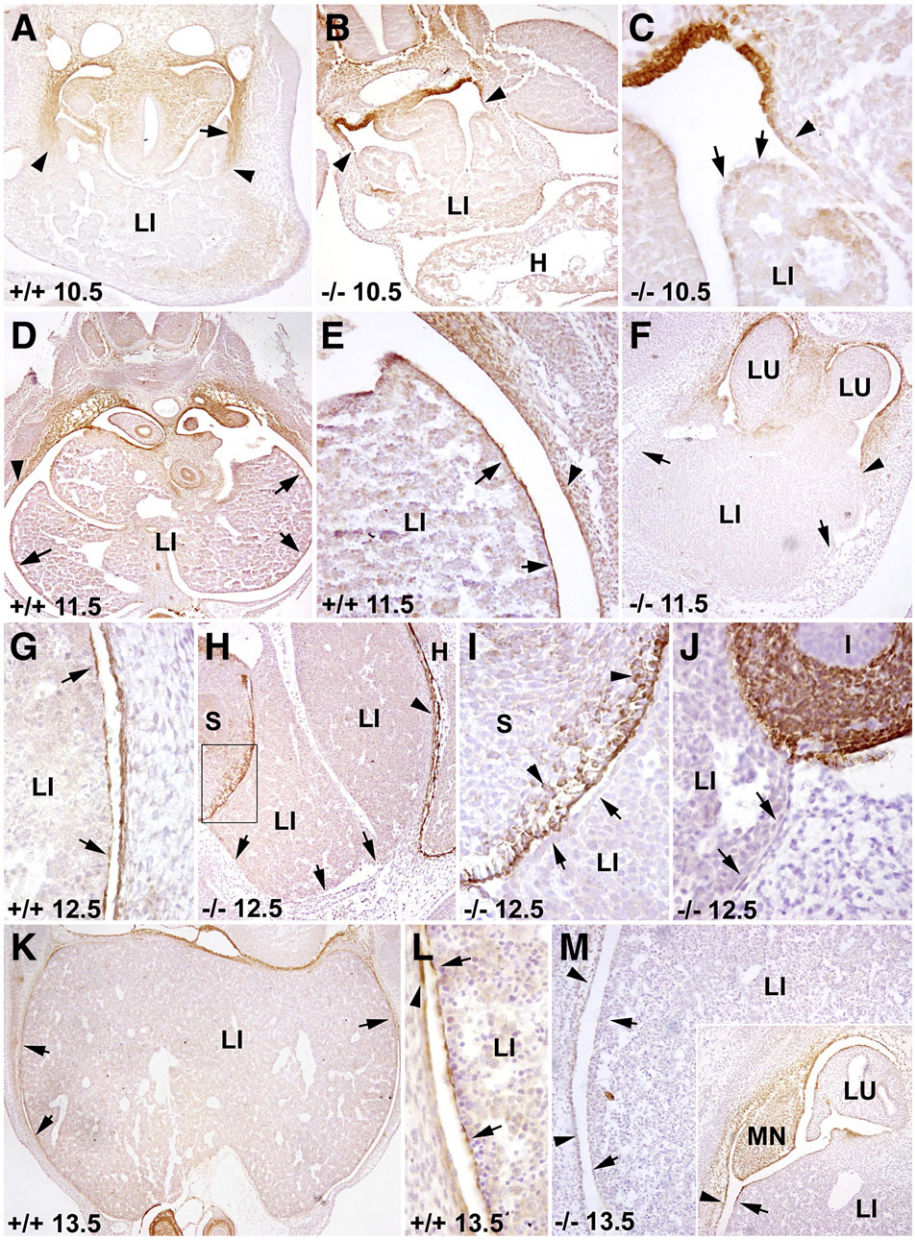

Fig. 6. RALDH2 expression in Wt1-null and control embryos. Hematoxylin counterstaining. (A–C) E10.5 control (A) and Wt1-null embryos (B, C) show moderate RALDH2 immunoreactivity in the dorsal lobes of the liver (arrows). In control embryos, immunoreactive cells can be seen extending through the dorsal and lateral walls of the coelomic cavity (arrowheads). However, in Wt1-null embryos, these cells remain closely associated to the dorsal coelomic epithelium (arrowheads). (D–F) E11.5 control (D, E) and Wt1-null (F) embryos already show important differences. Control embryos display RALDH2 immunoreactivity in the parietal (arrowheads) and liver (arrows) coelomic epithelia. However, Wt1-null embryos show no immunoreactivity in the lateral and ventral surface of the liver, and the limit of the parietal immunoreactivity remains in the same place as in the former stage (arrowhead in panel F). (G–J) Details of E12.5 control (G) and Wt1-null (H–J) embryos. Panel H show a sagittal section, and the box is shown at higher magnification in panel I. Control embryos show surface and parietal RALDH2 immunoreactivity (arrows in panel G), but in Wt1-null embryos the lateral and ventral liver surface is not stained (arrows), despite the strong immunoreactivity of the parietal pericardium (arrowhead in panel H) or other viscerae such as the stomach (S, arrowheads in panel I) or intestine (I) which serve as positive control. (K–M) E13.5 control (K, L) and Wt1-null (M) embryos. Immunoreactivity is weak but still visible in the liver surface and parietal epithelium of control embryos of this stage (arrows and arrowhead in panels K and L), but absent in Wt1-null littermates (arrows and arrowheads in panel M). The insert shows the dorsal area of the liver in the same section at lower magnification. The limit of the RALDH2-positive area of the parietal and visceral epithelia remains in the same place as in E10.5 embryos (arrowhead and arrow, respectively). Note staining in the rudimentary mesonephros (MN) and in the lung surface (LU).

the stomach. This is remarkable as the hepatic expression of Wt1 is restricted to the coelomic epithelium of the liver and to the cells delaminating from it. As soon as these delaminated cells disperse among the hepatoblasts, the expression of Wt1 is downregulated, as is the expression of cytokeratin and RALDH2. In contrast, the expression of other genes including GATA-4 and RXRα continues even as the cells differentiate into stellate cells and vascular smooth muscle cells. In addition, we identified a desmin-negative subpopulation of GATA-4- and RXRα-positive cells that is not incorporated into either the

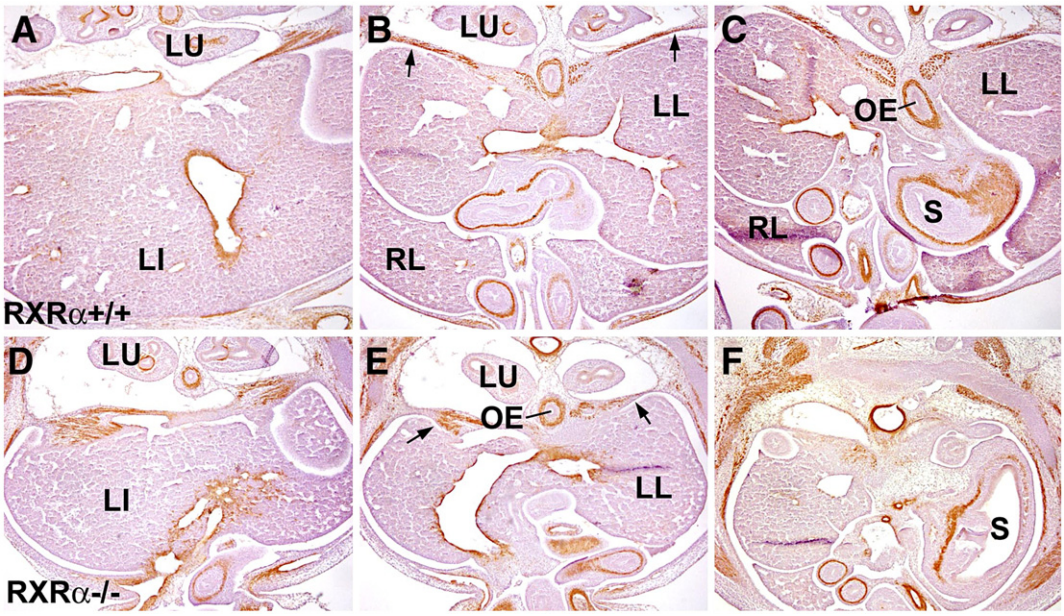

Fig. 7. Liver hypoplasia in E13.5 RXRα-null and control embryos. SMCα-actin immunostaining counterstained with hematoxylin. (A–C) Control embryo. (D–F) RXRα-null embryo. The mutant embryos have a smaller liver, especially the left lobe (LL). The stomach (S) is displaced to the left visceral cavity. The right liver lobe (RL) is also reduced. The mutant embryo shows a shortened and thinned diaphragm with disorganization of muscular cells (arrows).

sinusoids or vessels, and probably represents a progenitor pool of stellate/perivascular cells. Anyhow, the origin of stellate cells from coelomic epithelium-derived cells in mice seems well supported by our data, in agreement with our previous studies on avian embryos (Perez-Pomares et al., 2004), with reports on an origin of the stellate cells from the septum transversum mesenchyme (Enzan et al., 1997) and with the possibility raised by recent studies which discarded other sources (Cassiman et al., 2006).

GATA-4 is mainly expressed in the heart and endoderm (Bossard and Zaret, 1998), and thus its strong expression in coelomic cells and in stellate cell progenitors was unexpected. However, a recent study has shown that GATA-4 is required for liver and ventral pancreas development. Interestingly, in E9.5 embryos derived from GATA-4-deficient ES cells by tetraploid embryo complementation, the liver bud is able to form a pseudo-stratified epithelial liver but it fails to expand (Watt et al., 2007). These embryos lack septum transversum mesenchyme, thus suggesting the important role played by GATA-4 in the formation of this mesenchyme which appear to delaminate from the coelomic epithelium and is essential for liver bud growth. Similar observations have been made on GATA-6-deficient embryos (Zhao et al., 2005). Furthermore, Rojas et al. (2005) have described a GATA-4 enhancer which is strongly expressed in lateral mesoderm, septum transversum and perihepatic mesenchyme. The activity of this enhancer, which requires BMP4 signals and contains a high affinity Forkhead binding site, is maximum between E11.5 and E13.5, i.e. when we observe the delamination of GATA-4-positive cells from the surface of the liver and the formation of the stellate cell progenitor population. The lack of differences in the expression of GATA-4 in Wt1-null and control embryos suggests that this gene works upstream of Wt1 in liver development. All these observations can be related with the requirement of GATA-4 for development of the proepicardium (Watt et al., 2004), a coelomic outgrowth which is the progenitor tissue of the epicardium. We have shown elsewhere that the proepicardium is able to invade the liver and to supply it with sinusoidal cells (Perez-Pomares et al., 2004), thus suggesting common developmental potentials for GATA-4-expressing coelomic cells.

We attribute the liver phenotype of the Wt1-null embryos to two main factors; a reduction in hepatoblast proliferation at early stages, and the low proliferation and anomalous differentiation of the coelomic epithelium-derived cells that normally contribute to the stellate cell population (see Fig. 9 for our model). The differences in hepatoblast proliferation did not lead to a larger hepatoblast density in control embryos, as shown by HNF1 localization. Thus, this difference in proliferation should be related with the distal growth of the liver lobes, and thus with the final size and shape of the liver. On the other hand, the anomalous differentiation of the cells derived from the coelomic epithelium is evidenced by the altered expression pattern of SMC α-actin in Wt1-null embryos. Interestingly, stellate cells, even in adults, express low levels of SMC α-actin. During chronic liver disease, the expression of SMC α-actin increases dramatically, suggesting a myofibroblastic transformation of the stellate cells (Tsutsumi et al., 1987; Rockey et al., 1992; Enzan et al., 1994, 1995). We postulate that Wt1 represses the myofibroblastic transformation of the coelomic epithelium-derived cells, thus allowing for stellate cell differentiation.

At the molecular level, the sharp downregulation of RALDH2 expression in the coelomic epithelium lining the liver of Wt1-null mice probably underlies the proliferation and differentiation defects. Importantly, our results provide new evidence that similar mechanisms are involved in the development of the liver and the heart, since RALDH2 is also down-

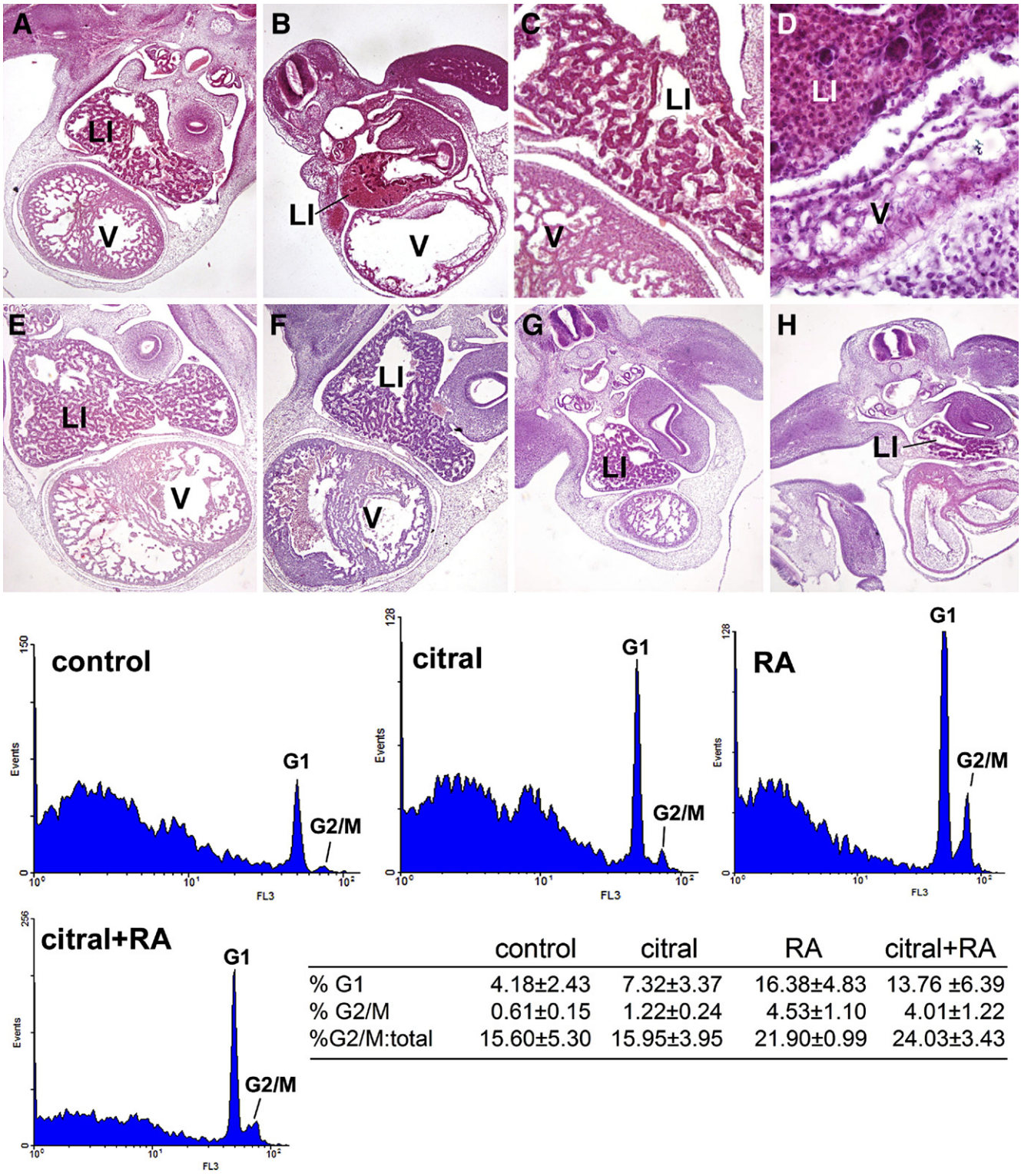

	control	citral	RA	citral+RA
% G1	4.18±2.43	7.32±3.37	16.38±4.83	13.76 ±6.39
% G2/M	0.61±0.15	1.22±0.24	4.53±1.10	4.01±1.22
%G2/M:total	15.60±5.30	15.95±3.95	21.90±0.99	24.03±3.43

Fig. 8. Inhibition of RA synthesis induces liver hypoplasia in chick embryos. (A–D) Severe liver hypoplasia is observed in chick embryos 48 h post treatment with DEAB at stage HH15. Treated embryos (B, D) show just a few hepatocytic clusters (arrows) surrounded by large blood-filled sinusoids. However, control embryos treated with DMSO show normal size livers (A, C). Note the hypoplasic heart ventricle (V) in panel B. (E–F) Treatment of embryos with DEAB by HH16, causes only a slight reduction in the liver size (F) as compared to the control embryos (E). (G–H) Treatment of HH15 embryos with citral, another competitive inhibitor of aldehyde dehydrogenases, induces the same phenotype as treatment with DEAB. The largest liver transverse sections of a citral-treated and a control embryo are shown in panels H and G, respectively. Bottom: Flow cytometry analysis of HH16–17 quail liver explants treated for 24 h with RA, citral, citral+RA or vehicle only. The experiment was performed by duplicate, but only one set of results is shown. Cells in G2/M are more abundant after RA treatments, but citral showed no significant effect. Note also the decrease in the abundance of subG1 cells (apoptotic and dead cells) with RA treatments. The table shows the area of the peaks as a percentage of the total area (mean±standard error of two experiments), as well as the percentage of G2/M cells respect to total cells (excluding the SubG1 fraction).

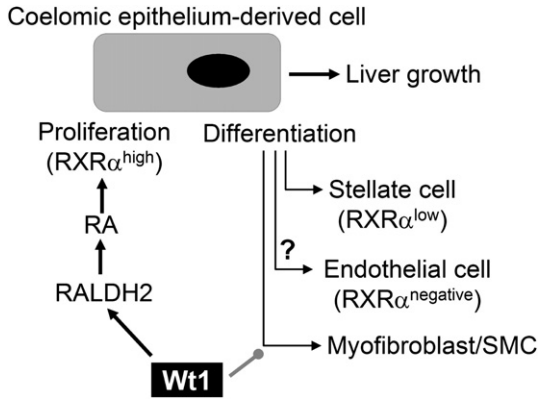

Fig. 9. Model of the function of Wt1 in hepatic development consistent with the results described in this paper. We propose that the coelomic epithelium-derived cells proliferate in response to RA/RXRα signals, promote liver growth, and differentiate into stellate cells, vascular smooth muscle and myofibroblasts. The possibility of a contribution to the sinusoid endothelial cells has also been suggested elsewhere (Moore et al., 1998; Perez-Pomares et al., 2004). According to our model, Wt1 regulates the expression of RALDH2 and represses the myofibroblastic/smooth muscle phenotype. Thus, loss of Wt1 leads to reduced proliferation of the coelomic epithelium-derived cell population (highly expressing RXRα cells), anomalous differentation into a myofibroblastic/smooth muscle cell phenotype and liver growth retardation. On the other hand, RXRα-null embryos would show only reduced liver growth, but no anomalous differentiation.

regulated in the epicardium of Wt1-null embryos (Pérez-Pomares et al., unpublished observations). In Wt1-null embryos, cells expressing high levels of RALDH2 are only found in a narrow band located in the dorsal part of the coelomic cavity, and no expression of RALDH2 is detected in the lateral and ventral areas of the developing liver. This could be significant, since it has been shown that waves of RALDH2 expression circulate throughout the embryo and contribute to the normal morphogenesis of the heart (Hochgreb et al., 2003). It is conceivable that Wt1 expression is required for the extension of a RALDH2 expression wave toward the lateral body wall and the liver, since the limit of the immunoreactive area remains always in the same place in Wt1-null embryos between E10.5 and E13.5 (Fig. 6). This would explain our results with quail liver explants in culture, where proliferation was low in isolated explants and the addition of an RA synthesis inhibitor had no significant effect. However, addition of RA to the medium, even in presence of the RA synthesis inhibitor citral, resulted in increased proliferation. Thus, the levels of RA in the immediate environment of the liver could be directly involved in the stimulation of liver growth and/or the induction of RALDH2 expression in the liver coelomic epithelium.

RA is an important morphogen, critical to the development of several organs. In the lung, RA promotes mesenchymal proliferation through the upregulation of Pdgf/PdgfRβ (Liebeskind et al., 2000) and FGF10 (Desai et al., 2004). Furthermore, it is essential for the proliferation of epicardially derived cells that secrete factors inducing myocardial proliferation (Kang and Sucov, 2005; Lavine et al., 2005). In the epicardium, expression of the RA receptor RXRα is essential not only for the proliferation of epicardially derived cells, but also for the production of a mitogenic signal for myocardial growth (Merki et al., 2005). The liver in both Wt1 and RXRα-null embryos is hypoplasic, the absence of the left lobe causing a malpositioning of the stomach. Both models display diaphragmatic defects, though RXRα-null embryos do not show any pleuroperitoneal defects. Interestingly, we did not observe any abnormal expression of SMC α-actin in the liver of RXRα-null embryos, suggesting that the proliferation of coelomic epithelium-derived cells, but not the differentiation, is dependent on RA signaling.

Our hypothesis that RA is required for normal liver growth, and thus that the observed loss of RALDH2 expression is causal to the liver phenotype, is further supported by our experiments with chick embryos. We were able to show that the inhibition of RALDH2 expression during the early stages of liver development (HH14–15) causes liver hypoplasia, whereas the same treatment at later stages of development (HH18) had no effect, suggesting that RA signaling is required during a very precise developmental window. Importantly, at these early stages, RALDH1 and RALDH3 are not expressed in the liver primordium (Blentic et al., 2003), hence inhibition of alternative endodermal RA synthesis pathways cannot account for the observed effect. The absence of hematopoietic cells in the avian liver by these stages dramatically showed that the hypoplasia was due to a reduction of the number of hepatoblasts. Strikingly, heart development was also affected by the treatment, as evidenced by epicardial defects and a thin ventricular myocardium, similar to the phenotype observed in Wt1-null and in RXRα-null embryos.

The relationship between the anomalous differentiation of coelomic epithelium-derived cells and hepatoblast proliferation remains obscure. However, it has been established that endothelial progenitors from the septum transversum are essential for liver morphogenesis (Matsumoto et al., 2001). Since these endothelial progenitors probably originate, like the stellate cells, from Wt1-expressing coelomic cells (Moore et al., 1998; Perez-Pomares et al., 2004), it is conceivable that the hepatic hypoplasia in Wt1-null embryos is related to the absence of trophic factors released by coelomic epithelium-derived cells before their differentiation into endothelial or stellate cells. In analogy, the LIM-homeobox gene *Lhx2* is expressed in the septum transversum and co-localizes with desmin, a main marker of stellate cells, in adult hepatic cells. Significantly, Lhx2-null embryos show normal differentiation of hepatocytes, but failure of liver growth, suggesting a role for stellate cells in promoting hepatoblast proliferation (Kolterud et al., 2004).

Two additional features of the liver phenotype in Wt1-null embryos are the decreased number of erythroblasts and the diaphragmatic defect. The impaired survival of hematopoietic cells observed in the Wt1-null embryos is possibly due to reduced erythropoietin (Epo) caused both by the loss of Wt1 expression and by the decrease in RALDH2 expression. Indeed, Epo has been shown to be a transcriptional target of Wt1 (Dame et al., 2006). Moreover, between E10 and E12, Epo expression in the liver is promoted by RA (Makita et al., 2001). As to the diaphragmatic defect, our data indicate this could be attributed to defective proliferation and differentiation of the transverse septum mesenchyme. Indeed, we observed abnormal accumulation of RALDH2+ cells at the site of the diaphragmatic

defect, suggesting a failure in the normal migration of these cells.

In summary, we describe a novel liver phenotype in Wt1-null mouse embryos. We show that Wt1 is required for the control of differentiation of the coelomic epithelium-derived stellate cell progenitor population, as well as for the activation/maintenance of a RA/RXRα signaling pathway essential for liver morphogenesis (summarised in Fig. 9). Importantly, mechanistic parallels can be drawn between liver, heart and gut (Wilm et al., 2005) development, suggesting a common and previously unsuspected role for the coelomic epithelium-derived cells in visceral development.

Acknowledgments

This work was supported by grants SAF2002-02651, BFU2005-00483 (Ministry of Education and Science, Spain), PI031159 (Ministry of Health, Spain), LST.CLG.980429 (Cooperative Science and Technology Sub-Programme, NATO), and LSHM-CT-2005-018630 (I+D Framework Programme VI, European Union). AIJ was supported by a European Union Marie Curie (FP5) personal fellowship, JAG by a Spanish Ministry of Education and Science fellowship and VPS by a fellowship from IP LSHM-CT-2005-018630 (I+D FP-VI, EU). We thank Dr. Daniel Metzger (IGBMC, Illkirch, France) and Dr. Peter McCaffery (Eunice Shriver Center-UMASS, USA) for the kind gifts of the RXRα-null embryos and the anti-RALDH2 antibody, respectively. The monoclonal antibodies QH1 and QCPN were obtained from the Developmental Studies Hybridoma Bank maintained by the Department of Pharmacology and Molecular Sciences, John Hopkins University School of Medicine, Baltimore, MD 21205, and the Department of Biological Sciences, University of Iowa, Iowa City, IA 52242, under contract NO1-HD-2-3144 from the NICHD.

References

Armstrong, J.F., Pritchard-Jones, K., Bickmore, W.A., Hastie, N.D., Bard, J.B., 1993. The expression of the Wilms' tumour gene, WT1, in the developing mammalian embryo. Mech. Dev. 40, 85–97.

Blentic, A., Gale, E., Maden, M., 2003. Retinoic acid signalling centres in the avian embryo identified by sites of expression of synthesising and catabolising enzymes. Dev. Dyn. 227, 114–127.

Bossard, P., Zaret, K.S., 1998. GATA transcription factors as potentiators of gut endoderm differentiation. Development 125, 4909–4917.

Cassiman, D., Barlow, A., Vander Borght, S., Libbrecht, L., Pachnis, V., 2006. Hepatic stellate cells do not derive from the neural crest. J. Hepatol. 44, 1098–1104.

Carmona, R., Macías, D., Guadix, J.A., Portillo, V., Pérez-Pomares, J.M., Muñoz-Chápuli, R., 2007. A simple technique of image analysis for specific nuclear immunolocalization of proteins. J. Microsc. 225, 96–99.

Dame, C., Kirschner, K.M., Bartz, K.V., Wallach, T., Hussels, C.S., Scholz, H., 2006. Wilms tumor suppressor, Wt1, is a transcriptional activator of the erythropoietin gene. Blood 107, 4282–4290.

Davies, R., Moore, A., Schedl, A., Bratt, E., Miyahawa, K., Ladomery, M., Miles, C., Menke, A., van Heyningen, V., Hastie, N., 1999. Multiple roles for the Wilms' tumor suppressor, WT1. Cancer Res. 59, 1747–1750.

Desai, T.J., Malpel, S., Flentke, G.R., Smith, S.M., Cardoso, W.V., 2004. Retinoic acid selectively regulates Fgf10 expression and maintains cell identity in the prospective lung field of the developing foregut. Dev. Biol. 273, 402–415.

Enzan, H., Himeno, H., Iwamura, S., Saibara, T., Onishi, S., Yamamoto, Y., Hara, H., 1994. Immunohistochemical identification of Ito cells and their myofibroblastic transformation in adult human liver. Virchows Arch. 424, 249–256.

Enzan, H., Himeno, H., Iwamura, S., Saibara, T., Onishi, S., Yamamoto, Y., Miyazaki, E., Hara, H., 1995. Sequential changes in human Ito cells and their relation to postnecrotic liver fibrosis in massive and submassive hepatic necrosis. Virchows Arch. 426, 95–101.

Enzan, H., Himeno, H., Hiroi, M., Kiyoku, H., Saibara, T., Onishi, S., 1997. Development of hepatic sinusoidal structure with special reference to the Ito cells. Microsc. Res. Tech. 39, 336–349.

Guadix, J.A., Carmona, R., Muñoz-Chapuli, R., Perez-Pomares, J.M., 2006. *In vivo* and *in vitro* analysis of the vasculogenic potential of avian proepicardial and epicardial cells. Dev. Dyn. 235, 1014–1026.

Herzer, U., Crocoll, A., Barton, D., Howells, N., Englert, C., 1999. The Wilms' tumor suppressor gene wt1 is required for development of the spleen. Curr. Biol. 9, 837–840.

Hochgreb, T., Linhares, V.L., Menezes, D.C., Sampaio, A.C., Yan, C.Y., Cardoso, W.V., Rosenthal, N., Xavier-Neto, J., 2003. A caudorostral wave of RALDH2 conveys anteroposterior information to the cardiac field. Development 130, 5363–5374.

Kang, J.O., Sucov, H.M., 2005. Convergent proliferative response and divergent morphogenic pathways induced by epicardial and endocardial signaling in fetal heart development. Mech. Dev. 122, 57–65.

Kastner, P., Grondona, J.M., Mark, M., Gansmuller, A., LeMeur, M., Decimo, D., Vonesch, J.L., Dolle, P., Chambon, P., 1994. Genetic analysis of RXR alpha developmental function, convergence of RXR and RAR signaling pathways in heart and eye morphogenesis. Cell 78, 987–1003.

Kolterud, A., Wandzioch, E., Carlsson, L., 2004. Lhx2 is expressed in the septum transversum mesenchyme that becomes an integral part of the liver and the formation of these cells is independent of functional Lhx2. Gene Expr. Patterns 4, 521–528.

Kreidberg, J.A., Sariola, H., Loring, J.M., Maeda, M., Pelletier, J., Housman, D., Jaenisch, R., 1993. WT-1 is required for early kidney development. Cell 74, 679–691.

Lavine, K.J., Yu, K., White, A.C., Zhang, X., Smith, C., Partanen, J., Ornitz, D.M., 2005. Endocardial and epicardial derived FGF signals regulate myocardial proliferation and differentiation in vivo. Dev. Cell 8, 85–95.

Le Douarin, N., 1975. An experimental analysis of liver development. Med. Biol. 53, 427–455.

Liebeskind, A., Srinivasan, S., Kaetzel, D., Bruce, M., 2000. Retinoic acid stimulates immature lung fibroblast growth via a PDGF-mediated autocrine mechanism. Am. J. Physiol.: Lung Cell. Mol. Physiol. 27, L81–L90.

Little, M., Holmes, G., Walsh, P., 1999. Wt1, what has the last decade told us? BioEssays 21, 191–202.

Makita, T., Hernandez-Hoyos, G., Chen, T.H., Wu, H., Rothenberg, E.V., Sucov, H.M., 2001. A developmental transition in definitive erythropoiesis, erythropoietin expression is sequentially regulated by retinoic acid receptors and HNF4. Genes Dev. 15, 889–901.

Matsumoto, K., Yoshitomi, H., Rossant, J., Zaret, K.S., 2001. Liver organogenesis promoted by endothelial cells prior to vascular function. Science 294, 559–563.

Merki, E., Zamora, M., Raya, A., Kawamaki, Y., Wang, J., Zhang, X., Burch, J., Kubalak, S.W., Kaliman, P., Izpisua-Belmonte, J.C., Chien, K., Ruiz-Lozano, P., 2005. Epicardial retinoid X receptor is required for myocardial growth and coronary artery formation. Proc. Natl. Acad. Sci. 102, 18455–18460.

Moore, A.W., Schedl, A., McInnes, L., Doyle, M., Hecksher-Sorensen, J., Hastie, N.D., 1998. YAC transgenic analysis reveals Wilms' tumour 1 gene activity in the proliferating coelomic epithelium, developing diaphragm and limb. Mech. Dev. 79, 169–184.

Moore, A.W., McInnes, L., Kreidberg, J., Hastie, N.D., Schedl, A., 1999. YAC complementation shows a requirement for Wt1 in the development of epicardium, adrenal gland and throughout nephrogenesis. Development 126, 1845–1857.

Pelletier, J., Bruening, W., Kashtan, C., Mauer, S., Manivel, J., Striegel, J.,

Houghton, D.C., Junien, C., Habib, R., Fouser, L., 1991. Germline mutations in the Wilms' tumor suppressor gene are associated with abnormal urogenital development in Denys-Drash syndrome. Cell 67, 437–447.

Perez-Pomares, J.M., Carmona, R., Gonzalez-Iriarte, M., Macias, D., Guadix, J.A., Muñoz-Chapuli, R., 2004. Contribution of mesothelium-derived cells to liver sinusoids in avian embryos. Dev. Dyn. 229, 465–474.

Pritchard-Jones, K., Fleming, S., Davidson, D., Bickmore, W., Porteous, D., Gosden, C., Bard, J., Buckler, A., Pelletier, J., Housman, D., 1990. The candidate Wilms' tumour gene is involved in genitourinary development. Nature 346, 194–197.

Rackley, R.R., Flenniken, A.M., Kuriyan, N.P., Kessler, P.M., Stoler, M.H., Williams, B.R., 1993. Expression of the Wilms' tumor suppressor gene WT1 during mouse embryogenesis. Cell Growth Differ. 4, 1023–1031.

Rockey, D.C., Boyles, J.K., Gabbiani, G., Friedman, S.L., 1992. Rat hepatic lipocytes express smooth muscle actin upon activation in vivo and in culture. J. Submicrosc. Cytol. Pathol. 24, 193–203.

Rojas, A., De Val, S., Heidt, A.B., Xu, S.M., Bristow, J., Black, B.L., 2005. Gata4 expression in lateral mesoderm is downstream of BMP4 and is activated directly by Forkhead and GATA transcription factors through a distal enhancer element. Development 132, 3405–3417.

Sharpe, J., Ahlgren, U., Perry, P., Hill, B., Ross, A., Heckser-Sorensen, J., Baldock, R., Davidson, D., 2002. Optical projection tomography as a tool for 3D microscopy and gene expression studies. Science 296, 541–545.

Sucov, H.M., Dyson, E., Gumeringer, C.L., Price, J., Chien, K.R., Evans, R., 1994. RXRα mutant mice establish a genetic basis for vitamin A signaling in heart morphogenesis. Genes Dev. 8, 1007–1018.

Tsutsumi, M., Takada, A., Takase, S., 1987. Characterization of desmin-positive rat liver sinusoidal cells. Hepatology 7, 277–284.

Watt, A.J., Battle, M.A., Li, J., Duncan, S.A., 2004. GATA4 is essential for formation of the proepicardium and regulates cardiogenesis. Proc. Natl. Acad. Sci. U. S. A. 101, 12573–12578.

Watt, A.J., Zhao, R., Li, J., Duncan, S.A., 2007. Development of the mammalian liver and ventral pancreas is dependent on GATA4. BMC Dev. Biol. 23 (7), 37.

Wilm, B., Ijpenberg, A., Hastie, N.D., Burch, J.B.E., Bader, D.M., 2005. The serosal mesothelium is a major source of smooth muscle cells of the gut vasculature. Development 132, 5317–5328.

Zhao, R., Watt, A.J., Li, J., Luebke-Wheeler, J., Morrisey, E.E., Duncan, S.A., 2005. GATA6 is essential for embryonic development of the liver but dispensable for early heart formation. Mol. Cell. Biol. 25, 2622–2631.